nature geoscience

ARTICLES

https://doi.org/10.1038/s41561-021-00812-2

A further source of Tokyo earthquakes and Pacific Ocean tsunamis

Jessica E. Pilarczyk[1,2,3]✉, Yuki Sawai[1], Yuichi Namegaya[1], Toru Tamura[1,4], Koichiro Tanigawa[1], Dan Matsumoto[1], Tetsuya Shinozaki[1], Osamu Fujiwara[1], Masanobu Shishikura[1], Yumi Shimada[1,5], Tina Dura[6], Benjamin P. Horton[7,8], Andrew C. Parnell[9] and Christopher H. Vane[10]

Earthquake hazard assessments for the Tokyo Region are complicated by the trench–trench triple junction where the oceanic Philippine Sea Plate not only underthrusts a continental plate but is also being subducted by the Pacific Plate. Great thrust earthquakes and associated tsunamis are historically recognized hazards from the Continental/Philippine Sea (Sagami Trough) and Continental/Pacific (Japan Trench) plate boundaries but not from the Philippine Sea/Pacific (Izu–Bonin Trench) boundary alone. Here we employed a series of historical and hypothetical rupture models to explain the widespread distribution of geological evidence for an unusually large tsunami found along 50 km of coastline east of Tokyo. Dating to about 1,000 years ago, this inferred tsunami predates local written history by several hundred years. We found that the inland extent of its sand sheet is best explained, in computer simulations, by displacement on one of the three plate boundaries offshore of the Boso Peninsula, which corresponds to the triple junction. The minimum magnitude scenario capable of generating the inland extent of inundation involves displacement along the Philippine Sea/Pacific boundary megathrust. This plate-boundary fault adds another potential source for earthquakes in the Tokyo Region and tsunamis in the Pacific Ocean.

The Tokyo metropolitan area and surrounding rural regions (Tokyo Region) are at risk from earthquakes and tsunamis that result from the triple junction of the Pacific (PAC), Philippine Sea (PHS) and Continental (CON) plates (Fig. 1a). The intersection of these plates produces three potential earthquake sources from three plate boundaries: CON/PHS (Sagami Trough), CON/PAC (Japan Trench) and PHS/PAC (Izu–Bonin Trench) (Fig. 1b,e). The third boundary, unconsidered until now as an independent source of large earthquakes, is thought to rupture only in combination with the CON/PAC boundary[1,2]. This assumption could lead to a misrepresentation of the seismic risk to the Tokyo Region. By assessing each of the three plate boundaries separately, it is possible to determine if, and at what minimum magnitude, each boundary may cause unusually large tsunami inundation along coastlines of the Tokyo Region.

Seismic risk associated with Tokyo's triple junction

Relative to the triple junction boundary located offshore of the Tokyo Region[3], there is an extensive history of earthquakes that originate from the CON/PHS and CON/PAC plate boundaries (Supplementary Fig. 1)[4,5]. CON/PHS boundary earthquakes have produced coseismically uplifted marine terraces along the southern tip of the Boso Peninsula near Tokyo, which are archived in a detailed 7,200-year record of past earthquakes[4]. The 2011 earthquake ruptured the northern and middle parts of the Japan Trench, and marked the largest rupture area (~600 km in length) of any known earthquake that previously originated from the CON/PAC plate boundary (Fig. 1e)[6,7]. Although unprecedented in size of rupture area, the 2011 earthquake tapered off well short of the triple junction[8] (Fig. 1e). Taking into consideration modelling and recently documented geological evidence, a repeat of a M 8–9 class earthquake along the CON/PAC plate boundary is not expected to occur for another ~550 to 1,100 years[5,9,10]. However, great uncertainty surrounds the seismic potential for the area surrounding the triple junction, including the PHS/PAC boundary, in the Tokyo Region[7,11].

Notable tsunamis that impacted the Tokyo Region in historical times include those on 31 December 1703 and 4 November 1677 CE. The 1703 CE Genroku earthquake and tsunami originated from at least the western part of the CON/PHS boundary (Fig. 1f and Supplementary Fig. 1) and produced widespread ground shaking[12]. The proximity of the rupture area to the Boso Peninsula produced ~6 m of localized uplift[4]. Along the eastern side of the Boso Peninsula, a subsequent tsunami ran inland ~2 km (ref. [13]). By contrast, the Empo earthquake of 1677 CE, the only known earthquake to have originated from a rupture that spans the CON/PAC and PHS/PAC plate boundaries[1,2,14], produced no uplift but generated a tsunami that inundated coastlines between southern Tohoku and the Boso Peninsula (Fig. 1f). Historical documents describe limited ground shaking on the Boso Peninsula and neighbouring Edo area (which corresponds to the area of modern-day Tokyo), but widespread damage associated with a tsunami several metres high[12]. Rupture models of this earthquake, constrained by historical records, do not account for the geometry of the triple junction. Although the models recognize PAC as the lower subducting plate,

[1]Geological Survey of Japan, National Institute of Advanced Industrial Science and Technology (AIST), Tsukuba, Japan. [2]Centre for Natural Hazards Research (CNHR), Department of Earth Sciences, Simon Fraser University, Burnaby, British Columbia, Canada. [3]Division of Marine Science, School of Ocean Science and Engineering, University of Southern Mississippi, Stennis Space Center, MS, USA. [4]Graduate School of Frontier Sciences, The University of Tokyo, Kashiwa, Japan. [5]Graduate School of Life and Environmental Sciences, University of Tsukuba, Tsukuba, Japan. [6]Department of Geosciences, Virginia Tech, Blacksburg, VA, USA. [7]Earth Observatory of Singapore, Nanyang Technological University, Singapore, Singapore. [8]Asian School of the Environment, Nanyang Technological University, Singapore, Singapore. [9]Hamilton Institute and Insight Centre for Data Analysis, Maynooth University, Kildare, Ireland. [10]British Geological Survey, Keyworth, UK. ✉e-mail: jessica_pilarczyk@sfu.ca

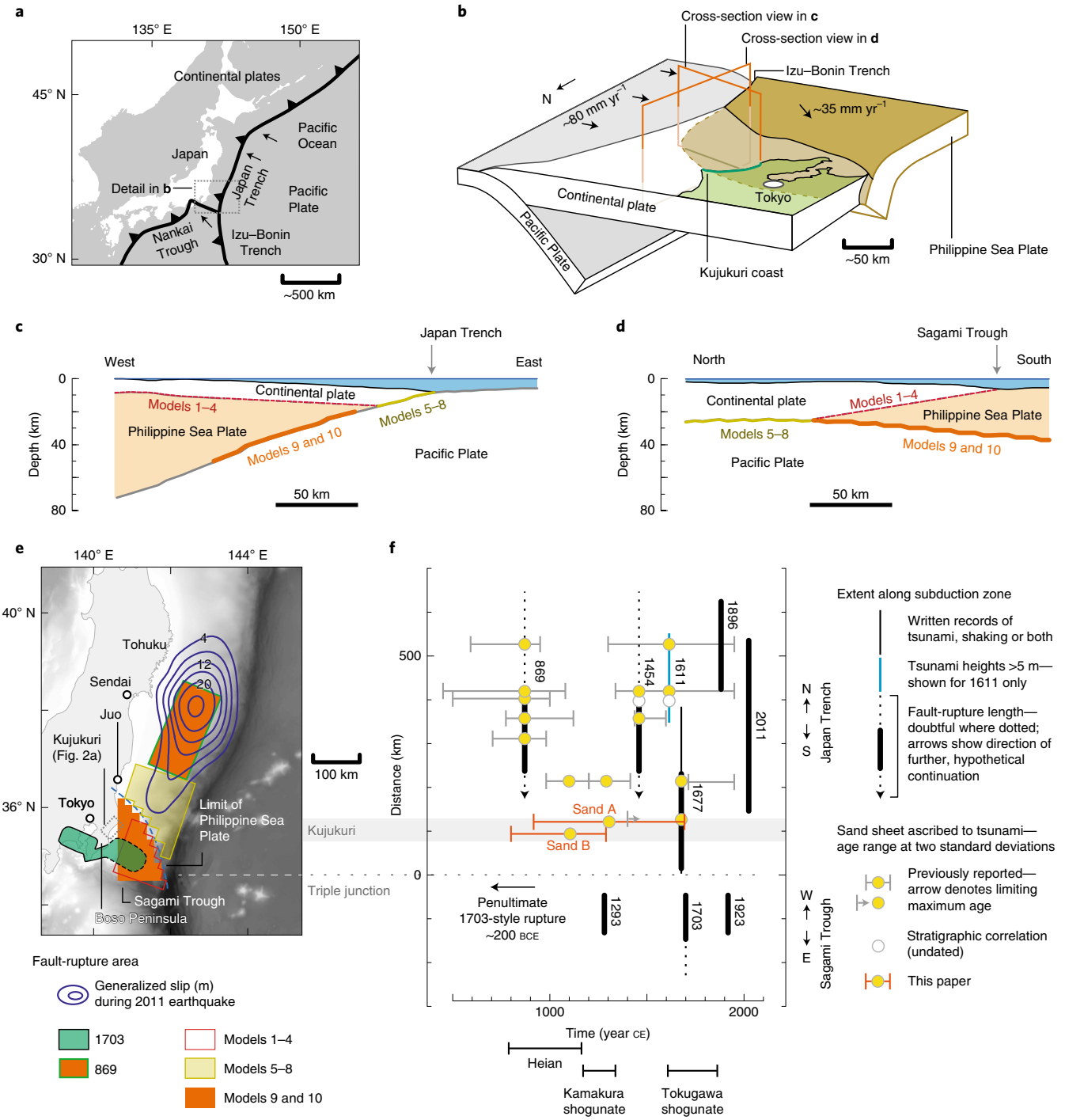

Fig. 1 | Location of the triple junction and associated historical and geological evidence for earthquakes along the three plate boundaries. a, Barbed lines show the seaward edge of the Japan Trench and Sagami Trough, and the arrows indicate plate motion. **b**, The block diagram depicts three earthquake sources, which result from the triple junction of the PAC, PHS and CON plates[25]. **c**,**d**, The modelled rupture area for all fault planes, which includes the rupture area responsible for sand B (model 10), is shown in the east–west (**c**) and north–south (**d**) orientations. The geometry of the plate boundaries refers to Nakajima and co-workers[26–28]. The earthquake source at the boundary between the PHS and PAC plates is indicated by an orange line. **e**, Northeastern Japan showing the rupture area of past CON/PAC (events in 869 CE[5] and 2011 CE[6]) and CON/PHS (event in 1703 CE[29]) earthquakes. The blue dashed line represents the boundary of the PHS plate[3]. Hypothetical earthquakes (models 10 and 11) that involve the subduction thrust along the PHS/PAC plate boundary explain the inland distribution of sand B (Fig. 2 and Supplementary Fig. 2). **f**, Geological evidence for plate boundary earthquakes and tsunamis. Horizontal error bars refer to the minimum and maximum radiocarbon ages for each reported sand sheet.

they do not differentiate between the two overriding plates, which hinders the assessment of the PHS/PAC boundary as a potential earthquake source[1,2,14].

Geological evidence for an unusually large tsunami

In the absence of instrumental or historical evidence of a third earthquake source, the PHS/PAC boundary, the geology along the

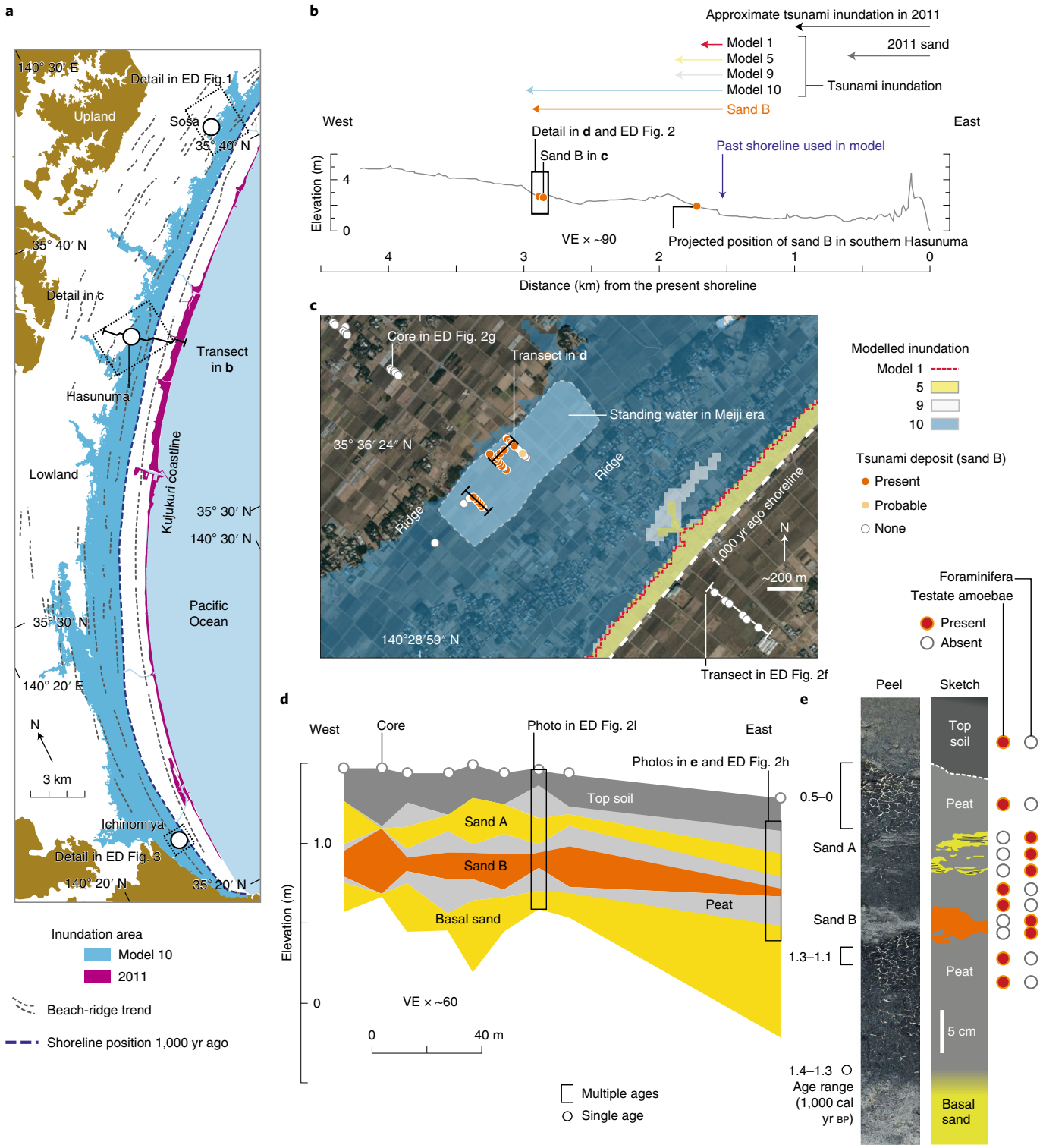

Fig. 2 | Stratigraphic and modelled evidence for a large tsunami about 1,000 years ago at Hasunuma in central Kujukuri. a, Index map showing the modern and palaeoshoreline from 1,000 years ago[16] relative to the 2011 Tohoku tsunami, and the modelled inundation (dark blue shaded area)[30]. **b**, Elevation profile for auger transect showing the inland extent of tsunami inundation (2011 Tohoku and models 1, 5, 9 and 10) relative to the sandy deposits associated with the 2011 Tohoku tsunami and sand B. **c**, Modelled inundation areas and shoreline position from 1,000 years ago at Hasunuma, central Kujukuri, relative to the coring sites. Photograph from the Geospatial Information Authority of Japan (https://maps.gsi.go.jp/development/ichiran.html). **d**, Stratigraphic cross-section of swales along the transect in **c**. **e**, Core photograph, sketch and microfossil data. Vertical exaggeration (VE) is indicated in **b** and **d**.

Kujukuri coastline, about 50 km east of Tokyo (Fig. 1e) was investigated. Indeed, the importance of using geological records in understanding a region's seismic risk was underlined when palaeoseismic evidence from Sendai revealed events in 869 and 1454 CE that could have forecast the severity of the Tohoku tsunami in 2011[5,10]. The Kujukuri coastline is characterized by a series of parallel and

Table 1 | Modelled scenarios, including hypothetical (models 1–11) and historical (models 12 and 13) earthquakes

Plate boundary	Modelled scenario			
CON/PHS	Model 1	Model 2	***Model 3***	***Model 4***
	Slip, 10 m	Slip, 15 m	Slip, 20 m	Slip, 25 m
	M_w 8.4	M_w 8.5	M_w 8.6	M_w 8.6
CON/PAC	Model 5	Model 6	Model 7	***Model 8***
	Slip, 10 m	Slip, 15 m	Slip, 20 m	Slip, 25 m
	M_w 8.5	M_w 8.7	M_w 8.7	M_w 8.8
PHS/PAC	Model 9	***Model 10***	-	-
	Slip, 5 m	Slip, 10 m		
	M_w 8.3	M_w 8.5		
PHS/PAC + CON/PAC	***Model 11***	-	-	-
	Slip, 10 m			
	M_w 8.7			
Jogan model (Namegaya and Satake, 2014)[23]	Model 12	-	-	-
	Slip, 12 m			
	M_w 8.6			
2011 Tohoku model (Fujii et al., 2011)[24]	Model 13	-	-	-
	Variable slip			
	M_w 9.0			

Model numbers in bold italics indicate scenarios that inundate sand B at the sampled field sites.

subparallel sandy beach ridges and swales that document a history of prograding shorelines over the last 5,500 years[15,16] (Fig. 2a). Swales between beach ridges previously produced detailed geological records of palaeotsunamis on the coastlines of Sumatra[17], Thailand[18] and Sendai[5] from the identification of anomalous sandy sediment that is incorporated into the coastal sedimentary record[5,18].

Two sand sheets buried beneath rice paddies were mapped at 142 locations along the Kujukuri coastline (Fig. 1a). At 47 of the investigated locations, two anomalous sands were traced in sedimentary sequences that spanned ~1,000 years. The chronology of the sedimentary sequences was constrained using 48 radiocarbon dates from freshwater peats under- and overlying the sands (Fig. 2 and Supplementary Tables 1 and 3). From young to old the sand deposits are labelled A (900–1700 CE) and B (800–1300 CE) (Extended Data Figs. 1–3 and Supplementary Tables 3–4). Sand A is found in most locations and extends up to 4 km inland of the modern shoreline. Synchronous traces of sand B extend up to 3.5 km inland, but are only found in central and southern Kujukuri (Extended Data Figs. 1–3). Sedimentary structures and palaeoecology indicate that sands A and B were deposited during high-energy marine inundation events. The sand layers range in thickness from 5 to 35 cm, have features consistent with tsunami deposits, such as a distinct erosional base, rip-up clasts, pebbles, normal grading and a mud drape, and are preserved along multiple sections of the 50-km-long stretch of coastline (Fig. 2). Marine foraminifera are present within the sand layers but not in the surrounding peat, mud or basal sand layers (Fig. 2e and Supplementary Table 2).

Possible historical earthquake sources for sand A include events in 1703 CE (CON/PHS earthquake) and 1677 CE (CON/PAC + PHS/PAC boundaries rupturing simultaneously), as well as an earlier undocumented event that is evidenced by sandy deposits at Juo (Fig. 1e,f)[5]. Sand B represents a previously undocumented event, falling within a time period for which Japanese earthquake historians have identified as having sparse written accounts[19] (Fig. 1f). The timing of sand B (~1,000 years ago) does not overlap with any instances of uplifted terraces along the Boso Peninsula (age discrepancy on the order of 700 to 1,200 years[20]), eliminating the western part of the CON/PHS plate boundary as the tsunami source for sand B. Given the uncertainty surrounding the subduction zone responsible for sand A (that is, two or more potential sources), modelling efforts were focused on sand B because its age and distribution may be explained by a previously unconsidered earthquake source along the PHS/PAC plate boundary.

Simulation models for the tsunami of 1,000 years ago

To resolve which boundaries have the potential to explain the inundation required to deposit sand B at Kujukuri, plausible minimum ruptures for 11 hypothetical fault models that involve earthquakes along the CON/PHS (models 1–4), CON/PAC (models 5–8), PHS/PAC (models 9–10) and CON/PAC and PHS/PAC (model 11, a combination of models 5 and 10) plate boundaries were used (Supplementary Fig. 2). Rather than reconstructing the specific earthquake (that is, rupture area and amount of slip) that generated the tsunami responsible for depositing sand B, minimum-slip rupture models were used to resolve which of the three plate boundaries is the most plausible candidate to have produced the tsunami inundation of 1,000 years ago (Table 1).

The palaeoshoreline position and height of the coastal dunes at the time of sand B's deposition were estimated using the average rate of shoreline progradation[16] and the height of the modern dunes. Multiple-slip scenarios for each fault plane were tested to determine the minimum earthquake magnitude along each of the three boundaries needed to explain the distribution of sand B (Table 1 and Supplementary Table 5). The models show that ruptures with less than 20 and 25 m of slip that occur on the CON/PHS and CON/PAC plate boundaries, respectively, are insufficient to generate tsunami inundation from the palaeoshoreline that would reach the landward limit of sand B (Supplementary Fig. 2). For example, model 7, based on a hypothetical plate boundary earthquake that occurs with 20 m slip along the CON/PAC plate boundary of the Japan Trench, produced inundation at Kujukuri that fell short of explaining the distribution of sand B at the sites we examined.

The minimum-slip scenarios that explain the distribution of sand B along the recognized CON/PHS and CON/PAC boundaries are models 3, 4 and 8. These modelled scenarios involve earthquakes with a large uniform slip in excess of 20 m. Given the wealth of historical and geological records that document CON/PHS and CON/PAC ruptures, it is not surprising that increasing the magnitude, and therefore slip, of CON/PHS and CON/PAC hypothetical ruptures ultimately results in widespread tsunami inundation along the Boso Peninsula. What is surprising, however, are models 10 and 11 with rupture areas that involve only 10 m of uniform slip along a previously unconsidered earthquake source. Model 10, the minimum rupture needed to explain the distribution of sand B, involves a M_w 8.5 earthquake that ruptures along the unconsidered PHS/PAC boundary. Model 11, a higher magnitude earthquake (M_w 8.7), which involves the combination of models 5 (CON/PAC) and 10 (PHS/PAC), also generated sufficient inundation. This scenario, similar to the suggested model of the 1677 CE earthquake[1,2,14], is speculative due to the lack of corroborating geological evidence in the southern Tohoku region, but provides compelling evidence for a PHS/PAC rupture that generates unusually large tsunami inundation along the Boso Peninsula. Geological evidence for the ~1.4 m of coseismic subsidence (model 11 in Supplementary Figure 2) predicted by the model was not detected in the study area due its distance from the shoreline. However, evidence for coseismic subsidence may be found in marshy areas closer to the shoreline, where abrupt changes in sea level can be detected by locating saltmarsh peat abruptly buried beneath tidal-to-subtidal sediments[21]. On the contrary, the minimal slip associated with lower magnitude ruptures (model 9) along the PHS/PAC plate boundary results in a smaller net vertical subsidence (~0.7 m) along the Kujukuri coast, which

mitigates inundation (Supplementary Fig. 2). Given the 1,000 year age range of sand B, the possibility exists that the Jogan rupture area (CON/PAC boundary offshore of the Sendai region) was potentially several hundred kilometres greater than previously thought and may have extended through the triple junction and generated widespread inundation that would have flooded extensive coastal areas from Tohoku to areas just east of Tokyo.

Is the Tokyo Region at risk of an earthquake and tsunami from a previously unconsidered source? As a precaution based on known recurrence intervals for the Japan Trench and Sagami Trough, seismic hazard maps of Japan identify the CON/PHS and CON/PAC plate boundaries as sources of large earthquakes, but omit the possibility that the PHS/PAC boundary could rupture independently of the other plate boundaries. Although seismic observations that span the past few decades capture small slip rates and no evidence for large earthquakes along the PHS/PAC boundary[3,22], these findings, based on a limited timeframe, do not deny the possibility that a larger rupture occurred in the past. Geological evidence for a tsunami that occurred about 1,000 years ago may be attributed to one of three plate boundaries that constitute Tokyo's triple junction, as five of the eleven modelled scenarios suggest a tsunami source in the area offshore of the Boso Peninsula. Among these are models 10 and 11, ruptures that involve the previously unconsidered PHS/PAC boundary. These inferred rupture areas add additional and potentially dangerous sources for earthquakes and tsunamis that threaten the Tokyo Region.

Online content

Any methods, additional references, Nature Research reporting summaries, source data, extended data, supplementary information, acknowledgements, peer review information; details of author contributions and competing interests; and statements of data and code availability are available at https://doi.org/10.1038/s41561-021-00812-2.

Received: 10 September 2018; Accepted: 14 July 2021;
Published online: 02 September 2021

References

1. *Committee for Subduction Zone Earthquakes in Japan and Kuril Trenches (10th Meeting)* [in Japanese] (Cabinet Office Japanese Government, 2005); http://www.bousai.go.jp/kaigirep/chuobou/senmon/nihonkaiko_chisimajishin/10/index.html
2. Takeuchi, H. et al. Survey of run-up height of Empo Boso-oki Earthquake Tsunami on the coast from Chiba Prefecture to Fukushima Prefecture (in Japanese with English abstract). *Rekishi Zishin* **22**, 53–59 (2007).
3. Uchida, N., Nakajima, J., Hasegawa, A. & Matsuzawa, T. What controls interplate coupling? Evidence for abrupt change in coupling across a border between two overlying plates in the NE Japan subduction zone. *Earth Planet. Sci. Lett.* **283**, 111–121 (2009).
4. Shishikura, M. History of the paleo-earthquakes along the Sagami Trough, central Japan: review of coastal paleo-seismological studies in the Kanto region. *Episodes* **37**, 246–257 (2014).
5. Sawai, Y., Namegaya, Y., Okamura, Y., Satake, K. & Shishikura, M. Challenges of anticipating the 2011 Tohoku earthquake and tsunami using coastal geology. *Geophys. Res. Lett.* **39**, L21309 (2012).
6. Ozawa, S. et al. Coseismic and postseismic slip of the 2011 magnitude-9 Tohoku-oki earthquake. *Nature* **475**, 373–376 (2011).
7. Simons, M. et al. The 2011 magnitude 9.0 Tohoku-Oki earthquake: mosaicking the megathrust from seconds to centuries. *Science* **332**, 1421–1425 (2011).
8. Satake, K., Fujii, Y., Harada, Y. & Namegaya, Y. Time and space distribution of coseismic slip of the 2011 Tohoku earthquake as inferred from tsunami waveform data. *Bull. Seismol. Soc. Am.* **103**, 1473–1492 (2013).
9. Satake, K. Geological and historical evidence of irregular recurrent earthquakes in Japan. *Philos. Trans. R. Soc. A* **373**, 20140375 (2015).
10. Sawai, Y., Namegaya, Y., Tamura, T., Nakashima, R. & Tanigawa, K. Shorter intervals between great earthquakes near Sendai: scour ponds and a sand layer attributable to AD 1454 overwash. *Geophys. Res. Lett.* **42**, 4795–4800 (2015).
11. Tormann, T., Enescu, B., Woessner, J. & Wiemer, S. Randomness of megathrust earthquakes implied by rapid stress recovery after the Japan earthquake. *Nat. Geosci.* **8**, 152–158 (2015).
12. Usami, T. et al. *Materials for Comprehensive List of Destructive Earthquakes in Japan 599–2012* (in Japanese) (Univ. Tokyo Press, 2013).
13. Watanabe, H. *Comprehensive List of Tsunamis to Hit the Japanese Islands* (in Japanese) (Univ. Tokyo Press, 1998).
14. Yanagisawa, H. et al. Tsunami earthquake can occur elsewhere along the Japan Trench—historical and geological evidence for the 1677 earthquake and tsunami. *J. Geophys. Res. Solid Earth.* **121**, 3504–3516 (2016).
15. Masuda, F., Fujiwara, O., Sakai, T. & Araya, T. Relative sea-level changes and co-seismic uplifts over six millennia, preserved in beach deposits of the Kujukuri strand plain, Pacific coast of the Boso Peninsula, Japan. *J. Geogr. (Chigaku zasshi)* **110**, 650–664 (2001).
16. Tamura, T., Murakami, F., Nanayama, F., Watanabe, K. & Saito, Y. Ground-penetrating radar profiles of Holocene raised-beach deposits in the Kujukuri strand plain, Pacific coast of eastern Japan. *Mar. Geol.* **248**, 11–27 (2008).
17. Monecke, K. et al. A 1,000-year sediment record of tsunami recurrence in northern Sumatra. *Nature* **455**, 1232–1234 (2008).
18. Jankaew, K. et al. Medieval forewarning of the 2004 Indian Ocean tsunami in Thailand. *Nature* **455**, 1228–1231 (2008).
19. Koyama, M. A review of historical seismology in Japan: analyses and proposals for next stage of study of historical documents. *J. Geogr.* **108**, 346–369 (1999).
20. Komori, J., Shishikura, M., Ando, R. & Yokoyama, Y. History of the great Kanto earthquakes inferred from the ages of Holocene marine terraces revealed by a comprehensive drilling survey. *Earth Planet. Sci. Lett.* **471**, 74–84 (2017).
21. Barlow, N. L. M. et al. Salt marshes as late Holocene tide gauges. *Glob. Planet. Change* **106**, 90–110 (2013).
22. Igarashi, T. Catalog of small repeating earthquakes for the Japanese Islands. *Earth Planets Space* **72**, 73 (2020).
23. Namegaya, Y. & Satake, K. Reexamination of the A.D. 869 Jogan earthquake size from tsunami deposit distribution, simulated flow depth, and velocity. *Geophys. Res. Lett.* **41**, 2297–2303 (2014).
24. Fujii, Y., Satake, K., Sakai, S., Shinohara, M. & Kanazawa, T. Tsunami source of the 2011 off the Pacific coast of Tohoku Earthquake. *Earth Planets Space* **63**, 815–820 (2011).
25. Wei, D. & Seno, T. in *Mantle Dynamics and Plate Interaction in East Asia* (eds Flower, M. et al.) 337–346 (American Geophysical Union, 1998).
26. Hirose, F., Nakajima, J. & Hasegawa, A. Three-dimensional velocity structure and configuration of the Philippine sea slab beneath Kanto district, central Japan, estimated by double-difference tomography. *J. Seismol. Soc. Jpn* **60**, 123–138 (2008).
27. Nakajima, J. & Hasegawa, A. Anomalous low-viscosity zone and linear alignment of seismicity along it in the subducted Pacific slab beneath Kanto, Japan: reactivation of subducted fracture zone? *Geophys. Res. Lett.* **33**, L16309 (2006).
28. Nakajima, J., Hirose, F. & Hasegawa, A. Seismotectonics beneath the Tokyo metropolitan area: effect of slab-slab contact and overlap on seismicity. *J. Geophys. Res.* **114**, B08309 (2009).
29. *Long-Term Evaluation of Subduction Zone Earthquakes around the Sagami Trough* (The Headquarters for Earthquake Research Promotion, 2004); https://www.jishin.go.jp/main/chousa/kaikou_pdf/sagami.pdf
30. *1:25,000 Tsunami Flood Area Overview Map* Technical Report D1-No. 592 (Geospatial Information Authority of Japan, 2011).

Methods

Sample collection and elevation survey. At central Kujukuri (Hasunuma) we conducted a detailed and extensive topographical survey. In northern (Sosa) and southern (Ichinomiya) Kujukuri we surveyed core locations (Supplementary Table 1 and Extended Data Figs. 1–3). Gouge coring documented stratigraphic changes at intervals no more than 50 m apart. Grain size, sedimentary structure, contacts, unit thickness and lateral and vertical facies changes were documented for correlation between the sites. After the expanded mapping of stratigraphy at each site, we selected the best locations to core for the detailed sampling of sedimentary layers for microfossil and radiocarbon analyses. To minimize the compaction and contamination of sediments during coring we used a 15 cm × 3 cm geoslicer to retrieve 1–3 m cores. One sliced sample at each site in Sosa and Ichinomiya, and six sliced samples at Hasunuma, were collected. The slices were subsampled at 1–2 cm for microfossil and radiocarbon analyses. Accurate measurements of the inland extent and height above sea level of sands A and B were determined by measuring the position of all the cores relative to Tokyo Peil (the mean sea level in Tokyo Bay) using a total station and real time kinematic satellite navigation system.

Microfossil analysis. Samples from cores retrieved from Sosa, Hasunuma and Ichinomiya were examined for foraminiferal (marine protist) and testate amoebae (freshwater protist) taxa. Approximately 5 cm^3 of sediment was sampled from targeted intervals within three cores[31]. Samples were wet sieved at >63 µm and examined in an aqueous medium under a binocular microscope. The total number of foraminifera present within 10 cm^3 of sediment was counted and is reported as the total concentration in Supplementary Table 2.

Chronology. For radiocarbon analysis, plant macrofossils and charcoal fragments were selected using a binocular microscope. The samples were first rinsed with distilled water to remove soil detritus and rootlets before analysis by accelerator mass spectrometry at the Beta Analytic Radiocarbon Laboratory in Florida. For calibration of the radiocarbon ages, we first used the radiocarbon-calibration program OxCal 4.3[32–34]. Age ranges (two standard deviations) were calculated using the calibration data of IntCal13 and Marine13[35] (Supplementary Tables 3 and 4). We used Bchron[36,37] and a bespoke Monte Carlo rejection sampling approach to calculate the timing of the deposition of sands A and B by relating them to their associated boundary radiocarbon ages (Supplementary Figs. 4 and 5).

A deposition-timing model was used on the same set of radiocarbon dates from cores obtained from rice paddies in Hasunuma and Ichinomiya. This Bayesian model calibrates all the radiocarbon dates and uses them as limiting constraints to estimate the ages of sands A and B (Supplementary Fig. 5). Derivation of the code is similar to that of Rubin et al.[38] and the code itself is available at https://github.com/andrewcparnell/sand_ages_pilarczyk. The model is fitted via rejection sampling[39], whereby a large number (50,000) of plausible ages are created, some of which are rejected due to the constraints of the radiocarbon dates and the law of superposition. The final set of accepted ages (24,999 in our model) can then be used as the posterior probability distribution of the ages of sands A and B. Highest density range estimates of 68.2 and 95.4% were created using the hdrcde package[40]. Plots were created using ggplot2[41].

Tsunami simulation modelling. We developed ten hypothetical fault models that involved earthquakes along the CON/PHS plate boundary (models 1–4), the CON/PAC plate boundary (models 5–8) and the PHS/PAC plate boundary (models 9 and 10) to assess whether they explain the distribution of sand B. An 11th hypothetical fault model (model 11) that involved both the PHS/PAC and CON/PAC plate boundaries rupturing at the same time was also used. We also tested published models for two historical and recent earthquakes: 869 CE Jogan (model 12) and 2011 CE Tohoku (model 13). Models 12 and 13 were run using the position of the Kujukuri shoreline of 1,000 years ago, the time when sand B was deposited.

For tsunami simulation development we: (1) computed vertical seafloor displacements from fault parameters (Supplementary Table 5) using Okada's equations[42], (2) solved non-linear shallow-water equations (linear equations in the coarsest grid area) in Cartesian coordinate systems based on Goto et al.[43] and (3) utilized a Manning's roughness coefficient of 0.03 $m^{-1/3}\,s^{-1}$. The rake angle was calculated from the relationship between the strike angle of the fault and the direction of the relative motion of the plates according to the model of Sella et al.[44]. Details for each of these parameters are summarized in Supplementary Table 5. Detailed and precise models of tsunami inundation at Kujukuri were obtained using a minimum grid spacing of 25 m for bathymetric (modified from J-EGG500 provided by the Hydrographic and Oceanographic Department, Japan Coast Guard/Japan Oceanographic Data Center) and topographic datasets. The first step of model development involved constructing a grid based on a detailed elevation–depth profile of the Kujukuri shelf and coastline using a combination of air photos, topographic maps and a 5 m grid (a 10 m grid was used in a small section outside of the inundation zone) digital elevation model from the Geospatial Information Authority of Japan. The second step involved constraining the age of each tsunami associated with sands A and B, and using the palaeotopographical reconstructions of Tamura et al.[45] to estimate the position of the Kujukuri coastline and height of the barrier at the time sand B was deposited. The palaeoshoreline of 1,000 years ago is estimated to be 1 km inland of the current shoreline[45] and it is assumed that the height of the palaeobarrier is the same as that of the present day dunes.

Our simulations spanned a time period of 6 h from the time of the modelled rupture to account for all the possible tsunami propagations. The modelled inundations for each scenario (Supplementary Fig. 2) were compared with the inland extent of each candidate tsunami deposit to determine which, if any, simulation explains their occurrence.

The free software package, Generic Mapping Tools (GMT)[46], was used to draw the index maps in Figs. 1 and 2, and Extended Data Figs. 1–3. GEBCO 2020 was used for the bathymetric data in Fig. 1e and Supplementary Figs. 1 and 2[47].

Data availability

All data integral to the stated conclusions are presented within the paper, extended data and Supplementary Information. Data tables can be accessed at https://doi.org/10.5281/zenodo.5056915.

Code availability

Code for the Bayesian model can be accessed at https://github.com/andrewcparnell/sand_ages_pilarczyk.

References

31. Pilarczyk, J. E. et al. Microfossils from coastal environments as indicators of paleo-earthquakes, tsunamis and storms. *Palaeogeogr. Palaeoclimatol. Palaeoecol.* **413**, 144–157 (2014).
32. Bronk Ramsey, C. Radiocarbon calibration and analysis of stratigraphy: the OxCal program. *Radiocarbon* **37**, 425–430 (1995).
33. Bronk Ramsey, C. Development of the radiocarbon program OxCal. *Radiocarbon* **43**, 355–363 (2001).
34. Bronk Ramsey, C. & Lee, S. Recent and planned developments of the program OxCal. *Radiocarbon* **55**, 720–730 (2013).
35. Reimer, P. J. et al. IntCal13 and Marine13 radiocarbon age calibration curves 0–50,000 years cal BP. *Radiocarbon* **55**, 1869–1887 (2013).
36. Haslett, J. & Parnell, A. A simple monotone process with application to radiocarbon-dated depth chronologies. *J. R. Stat. Soc. C* **57**, 399–418 (2008).
37. Parnell, A., Haslett, J., Allen, J., Buck, C. & Huntley, B. A flexible approach to assessing synchroneity of past events using Bayesian reconstructions of sedimentation history. *Quat. Sci. Rev.* **27**, 1872–1885 (2008).
38. Rubin, C. et al. Highly variable recurrence of tsunamis in the 7,400 years before the 2004 Indian Ocean tsunami. *Nat. Commun.* **8**, 16019 (2017).
39. Robert, C. & Casella, G. *Introducing Monte Carlo Methods with R* (Springer, 2010).
40. Hyndman, R. *hdrcde: Highest Density Regions and Conditional Density Estimation* (pkgdown, 2018); http://pkg.robjhyndman.com/hdrcde
41. Wickham, H. *Ggplot2: Elegant Graphics for Data Analysis* (Springer, 2016).
42. Okada, Y. Surface deformation due to shear and tensile faults in a half-space. *Bull. Seismol. Soc. Am.* **75**, 1135–1154 (1985).
43. Goto, C., Ogawa, Y., Shuto, N. & Imamura, F. *IUGG/IOC Time Project, Numerical Method of Tsunami Simulation with the Leap-Frog Scheme* IOC Manuals and Guides 35 (UNESCO, 1997).
44. Sella, G. F., Dixon, T. H. & Mao, A. REVEL, a model for recent plate velocities from space geodesy, *J. Geophys. Res. B* https://doi.org/10.1029/2000JB000033 (2002).
45. Tamura, T., Murakami, F. & Watanabe, K. Holocene beach deposits for assessing coastal uplift of the northeastern Boso Peninsula, Pacific coast of Japan. *Quatern. Res.* **74**, 227–234 (2010).
46. Wessel, P., Smith, W. H. F., Scharroo, R., Luis, J. & Wobbe, F. Generic Mapping Tools: improved version released. *EOS Trans. AGU* **94**, 409–410 (2013).
47. GEBCO Bathymetric Compilation Group *The GEBCO_2020 Grid—A Continuous Terrain Model of the Global Oceans and Land* (British Oceanographic Data Centre, 2020); https://doi.org/10.5285/a29c5465-b138-234d-e053-6c86abc040b9

Acknowledgements

We thank B. Atwater, K. Satake and K. Ioki for their comments on an earlier version of the manuscript. This work is a contribution to IGCP Project 725, was supported by the Geological Survey of Japan, National Institute of Advanced Industrial Science and Technology (AIST) and in part by grants awarded to J.E.P. (National Science Foundation (EAR-1303881 and 1624612), Natural Sciences and Engineering Council of Canada (NSERC), Canada Research Chair (CRC) program and Japan Society for the Promotion of Science (JSPS) International Research Fellows (Geological Survey of Japan, AIST, PE14038)), A.C.P. (Science Foundation Ireland Career Development Award (17/CDA/4695), Investigator Award (16/IA/4520), Marine Research Programme funded by the Irish Government, co-financed by the European Regional Development Fund (Grant-Aid Agreement no. PBA/CC/18/01), European Union's Horizon 2020 research and innovation programme under grant agreement no. 818144 and SFI Research Centre (16/RC/3872 and 12/RC/2289_P2)) and B.P.H. (Singapore Ministry of Education Academic Research Fund (MOE2019-T3-1-004), National Research Foundation

Singapore and Singapore Ministry of Education, under the Research Centers of Excellence initiative). This work is Earth Observatory of Singapore contribution 382. CT scanning (Fig. ED2I) was performed under the cooperative research programme of the Center for Advanced Marine Core Research (CMCR), Kochi University (no. 17A008). C.H.V. publishes with the permission of the Executive Director British Geological Survey.

Author contributions

This project was led by Y. Sawai and J.E.P. J.E.P. led the writing of the main text, with contributions from the other authors. Y. Sawai led the fieldwork and prepared the figures and tables. Y.N. ran the simulated tsunami inundation models. T.T., Y. Sawai and Y.N. reconstructed the palaeoshoreline. J.E.P. conducted the microfossil analysis, C.H.V. and B.P.H. assisted with the stratigraphic interpretations, Y. Sawai, Y. Shimada and K.T. selected samples for radiocarbon dating and A.C.P. conducted the Bayesian statistical analyses and generated an age-depth model. Y. Sawai, J.E.P., Y.N., T.T., K.T., D.M., T.S., O.F., M.S., Y. Shimada and T.D. were involved in the fieldwork.

Competing interests

The authors declare no competing interests.

Additional information

Extended data is available for this paper at https://doi.org/10.1038/s41561-021-00812-2.

Supplementary information The online version contains supplementary material available at https://doi.org/10.1038/s41561-021-00812-2.

Correspondence and requests for materials should be addressed to J.E.P.

Peer review information Primary Handling editors: Stefan Lachowycz, Rebecca Neely, and Melissa Plail, in collaboration with the *Nature Geoscience* team. *Nature Geoscience* thanks Takuya Nishimura and the other, anonymous, reviewer(s) for their contribution to the peer review of this work.

Reprints and permissions information is available at www.nature.com/reprints.

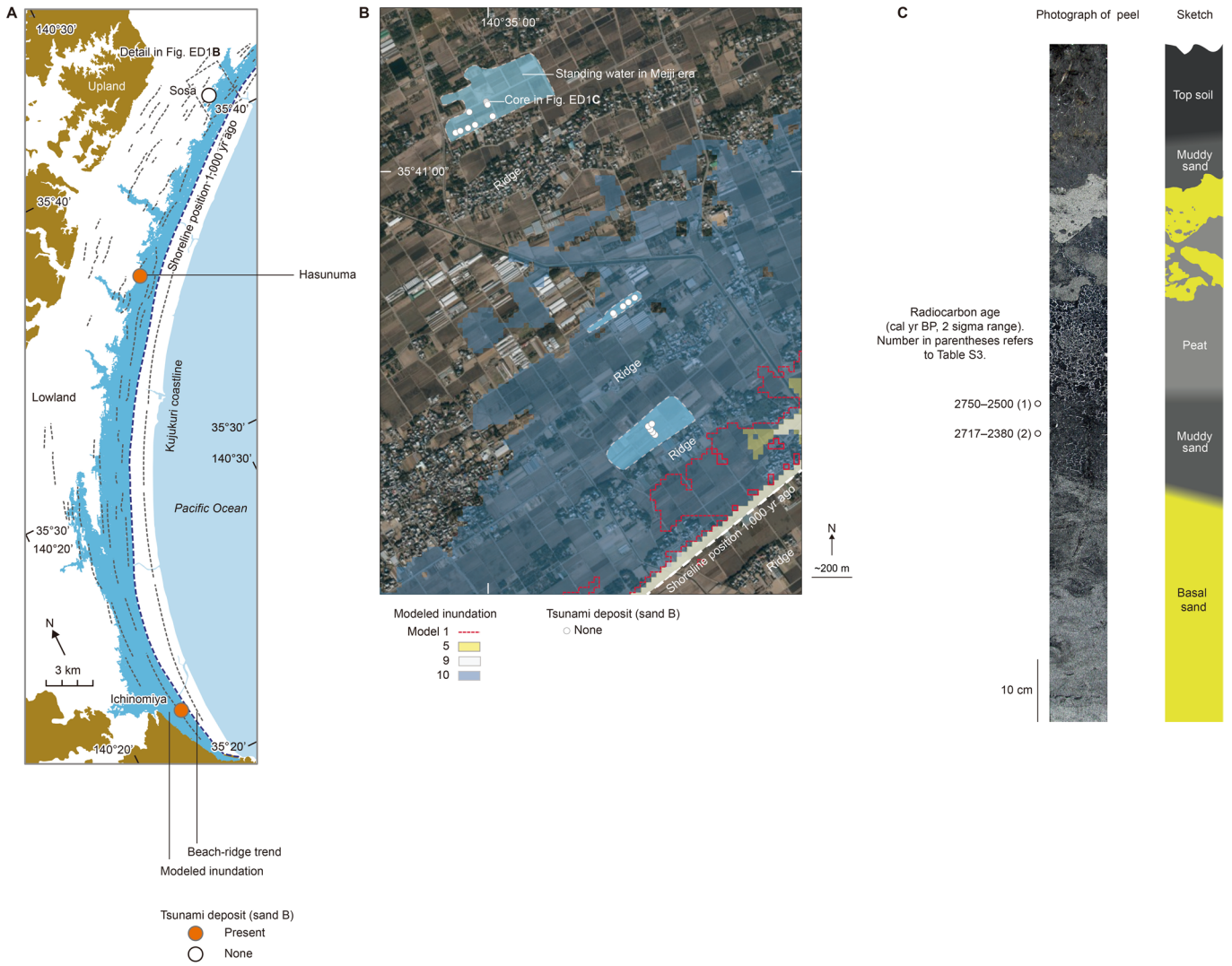

Extended Data Fig. 1 | Evidence for large-scale tsunami inundation at Sosa (north Kujukuri). a, Modelled inundation at Kujukuri relative to the position of sand B. Index map, showing geomorphology, position of tsunami deposits (sand B), and inundation area estimated from model 10 for all three field sites in Sosa, Hasunuma, and Ichinomiya (Supplementary Fig. 2). **b**, Modelled inundation at Sosa (north Kujukuri) relative to the position of sand B. Core locations at Sosa relative to inundation resulting from models 1 (red line), 5 (yellow shaded area), 9 (white shaded area), and 10 (sky blue shaded area). Sky blue areas bounded by a dashed line represent the location of past reservoirs or ponds that are evident in historical maps from the Meiji era (c. 1868–1922 CE). Photograph from the Geospatial Information Authority of Japan (GSI; https://maps.gsi.go.jp/development/ichiran.html). **c**, Stratigraphic evidence for a tsunami at Sosa (north Kujukuri). Photograph and stratigraphic log of core shown in **b**.

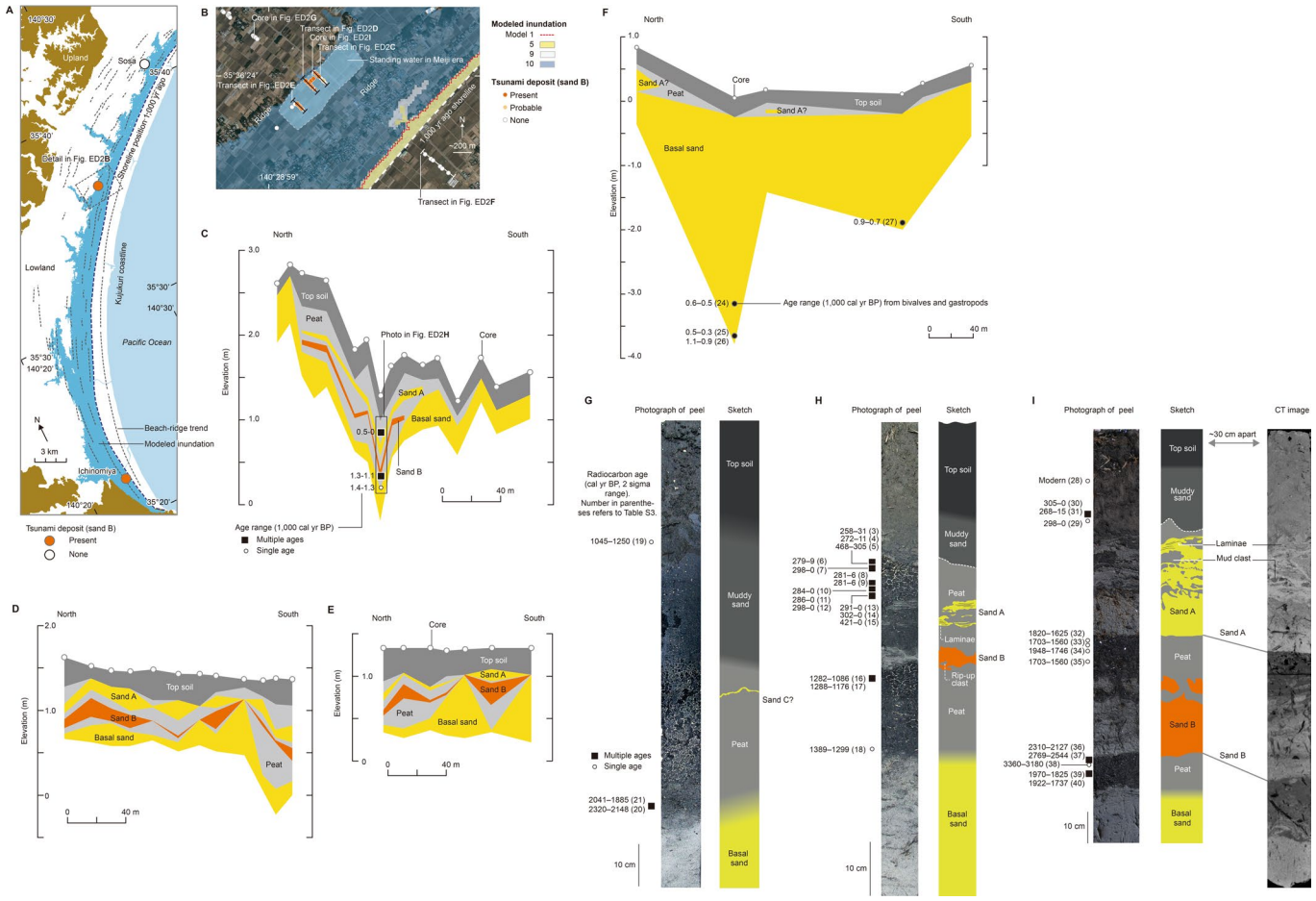

Extended Data Fig. 2 | Evidence for large-scale tsunami inundation at Hasunuma (central Kujukuri). a, Modelled inundation at Kujukuri relative to the position of sand B. Index map, showing geomorphology, position of tsunami deposits (sand B), and inundation area estimated from model 10 for all three field sites in Sosa, Hasunuma, and Ichinomiya (Supplementary Fig. 2). **b**, Modelled inundation at Hasunuma (central Kujukuri) relative to the position of sand B. Core locations at Hasunuma relative to inundation resulting from models 1 (red line), 5 (yellow shaded area), 9 (white shaded area), and 10 (sky blue shaded area). Sky blue areas bounded by a dashed line represent the location of past reservoirs or ponds that are evident in historical maps from the Meiji era (c. 1868–1922 CE). Photograph from Geospatial Information Authority of Japan (GSI; https://maps.gsi.go.jp/development/ichiran.html). **c–f** Stratigraphic evidence for two tsunamis at Hasunuma (central Kujukuri). Detailed cross section of stratigraphy from transect shown in **b**. **g**-**h**, Stratigraphic evidence for two tsunamis at Hasunuma (central Kujukuri). Photograph and stratigraphic log of core shown in **c**. **i**, Stratigraphic evidence for two tsunamis at Hasunuma (central Kujukuri). Photograph, stratigraphic log, and CT image of core shown in **b**.

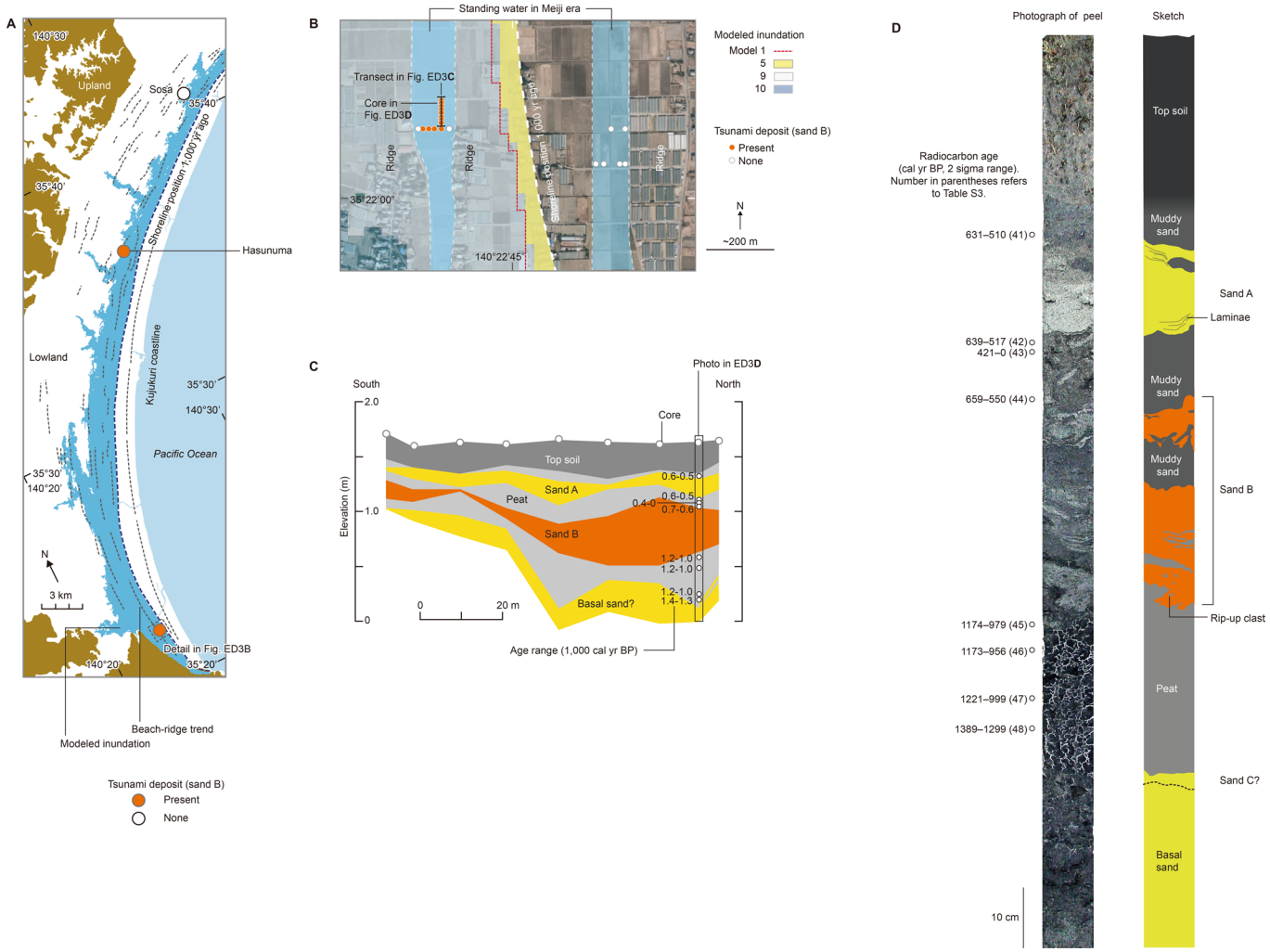

Extended Data Fig. 3 | Evidence for large-scale tsunami inundation at Ichinomiya (south Kujukuri). a, Modelled inundation at Kujukuri relative to the position of sand B. Index map, showing geomorphology, position of tsunami deposits (sand B), and inundation area estimated from model 10 for all three field sites in Sosa, Hasunuma, and Ichinomiya (Supplementary Fig. 2). **b**, Modelled inundation at Ichinomiya (south Kujukuri) relative to the position of sand B. Core locations at Ichinomiya relative to inundation resulting from models 1 (red line), 5 (yellow shaded area), 9 (white shaded area), and 10 (sky blue shaded area). Sky blue areas bounded by a dashed line represent the location of past reservoirs or ponds that are evident in historical maps from the Meiji era (c. 1868–1922 CE). Photograph from Geospatial Information Authority of Japan (GSI; https://maps.gsi.go.jp/development/ichiran.html). **c**, Stratigraphic evidence for two tsunamis at Ichinomiya (south Kujukuri). Detailed cross section of stratigraphy from transect shown in **b**. **d**, Stratigraphic evidence for up to three tsunamis at Ichinomiya (south Kujukuri). Photograph and stratigraphic log of core shown in **b**, **c**.